4D hyperspectral imaging for intraoperative tissue classification

Narek Chilingaryan[a], Fernando Villarruel[a], Tigran Soghomonyan[a], Varduhi Yeghiazaryan[b], and Narine Sarvazyan[a,b,c]

[a]L. A. Orbeli Institute of Physiology NAS RA, Yerevan, Armenia
[b]American University of Armenia, Yerevan, Armenia
[c]George Washington University, Washington, DC, United States

ABSTRACT

This study examines the use of 4D hyperspectral imaging (4D HSI) for visualizing clinically relevant targets. The approach relies on intrinsic optical properties of the tissue without the need for exogenous dyes or contrast agents. We compare autofluorescence-based 4D HSI to a traditional 3D HSI approach for its ability to distinguish between nerve and ligament bundles, isolated from adult cow trotters. Datacubes are captured within the 420–720 nm interval, under illumination wavelengths ranging from 300 to 400 nm. The unmixing outcomes of individual 3D HSI cubes prove inferior to those from multiple, even as few as three, 3D cubes sequentially combined into one. The data show an increase in the ratio of correctly identified pixels with the increased number of HSI cubes taken at different excitation wavelengths. Combining multiple 3D HSI cubes into a single 4D dataset improves target identification and reveals additional features, such as damaged nerve with torn epineurium. The 4D HSI approach merges excitation–emission matrices with traditional HSI and delivers higher accuracy in distinguishing different tissue structures. Furthermore, more advanced analysis techniques, such as deep neural networks, can potentially utilize 4D HSI data further to distinguish surgical targets. The data suggest that 4D HSI has significant potential for various clinical applications, including surgical procedures, dental applications, and cancerous lesion identification, leveraging small spectral changes for improved visualization and clinical outcomes.

Keywords: 4D hyperspectral imaging, excitation–emission matrices, surgery, nerve identification

1. INTRODUCTION

This study builds upon earlier efforts by us and others to use the intrinsic optical properties of tissues for visualization of clinically relevant targets without the need for exogenous dyes or contrast agents.[1–4] We explore the advantages of the 4D hyperspectral imaging (4D HSI) modality that collects and processes data acquired from both excitation and emission axes. Recent advances in optics, such as fast tunable light sources and snapshot cameras, made the 4D HSI approach suitable for intraoperative monitoring of the surgical field-of-view. Each 4D HSI dataset contains values from four axes: two spatial dimensions (x and y) and two spectral dimensions (excitation and emission wavelengths, λ_{ex} and λ_{em}). This study compares the performance of autofluorescence-based 4D HSI to the traditional emission-based 3D HSI approach. Excised bovine nerve and ligament bundles were used as examples of targets to be distinguished to allow avoiding inadvertent nerve damage during surgery. Such damage can result from inter-patient anatomical variability and visual similarity of nerve fibers to nearby structures, posing significant risks, including loss of sensation and paralysis.[5] This study highlights the potential of the 4D HSI approach as a promising candidate for developing new imaging methods to distinguish nerves intraoperatively.

Medical Imaging 2025: Clinical and Biomedical Imaging, edited by Barjor S. Gimi, Andrzej Krol, Proc. of SPIE Vol. 13410, 134100Z · © 2025 SPIE
1605-7422 · doi: 10.1117/12.3047177

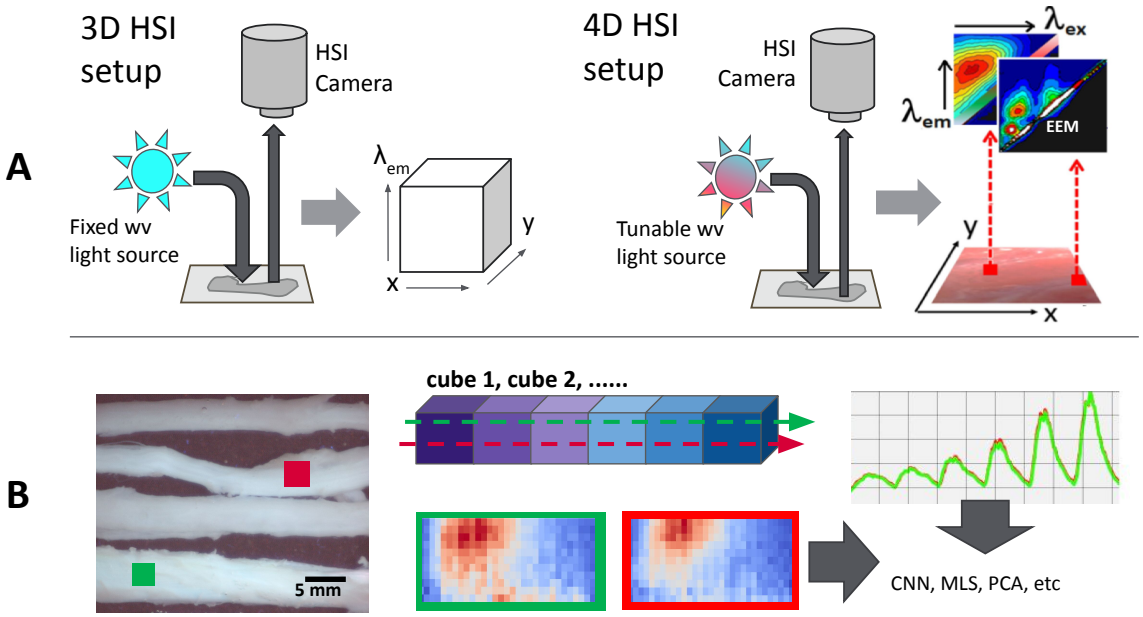

Figure 1: Schematics of experimental design. A. Traditional emission-based 3D HSI setup includes light source at fixed illumination wavelength followed by acquisition of grayscale images at specified emission wavelengths. It yields a 3D dataset called HSI cube with x, y and λ_{em} coordinates. In case of 4D HSI, the wavelength of excitation light also varies leading to a 4D dataset with x, y, λ_{em} and λ_{ex} coordinates. From each (x, y) pixel the excitation–emission matrix can be then extracted. B. Snapshot showing example of regions of interest (ROIs) placed on the image of excised target tissues. From each ROI or a pixel either a sequence of spectral profiles or an EEM can be extracted and analyzed by a variety of computational means. This report considers a linear arrangement of multiple 3D cubes, while a companion paper[6] applies CNN using EEMs as images.

2. MATERIALS AND METHODS

Hyperspectral datasets (available at https://zenodo.org/communities/nar-sar-iph/) were acquired from bovine trotters obtained from a local abattoir. Following dissection, the specified nerve and ligament segments were kept in medical-grade saline (0.9%) before and during image acquisition. To illuminate samples at different wavelengths, a TLS130B-300X tunable light source (Newport Corp, NJ) with a 77776 focusing lens assembly was used to maximize light output (Fig. 1A). Light was directed toward the samples using a mirror. The tested illumination wavelengths ranged from 300 to 400 nm, at either 5 or 10 nm steps. The Nuance FX imaging system (model: N-MSI-FX, CRi, Woburn, MA, USA) was used for hyperspectral data acquisition, with each datacube captured at 10 nm steps within the 420–720 nm wavelength interval. Image processing was performed using a combination of the proprietary Nuance 3.0.2 software[3] and a custom-written Python script. Region of interest (ROI)-based linear unmixing was applied to individual 3D HSI cubes or to a sequential combination of multiple 3D HSI cubes (three, six or eleven cubes) stitched into a single 4D HSI dataset (Fig. 1B). A companion paper[6] discusses the application of deep convolutional neural networks (CNN) to unmix these 4D HSI datasets, treating excitation–emission matrices (EEM) extracted from each spectral pixel as images. The unmixing outcomes were assessed both visually and numerically using the component images produced by the software (Fig. 2B). For numerical assessment, the component images were analyzed with two different approaches. Masks with

Further author information: (Send correspondence to N.S.)
N.Ch.: narek.chilingaryan@physiol.sci.am F.V.: villarruel.fernando@physiol.sci.am
T.S.: tsoghomonyan@physiol.sci.am V.Y.: vyeghiazaryan@aua.am N.S.: phynas@gwu.edu

classification labels were generated based on maximum-value-component at each pixel position, then compared to manually generated reference masks to obtain overall accuracy scores (Fig. 3A). Also, for each segment of the reference mask, component averages and their ratios were calculated as a proposed measure for unmixing evaluation per class (Fig. 2C and Fig. 3B). Friedman test was used to compare the accuracy results for statistical significance.

3. RESULTS AND DISCUSSION

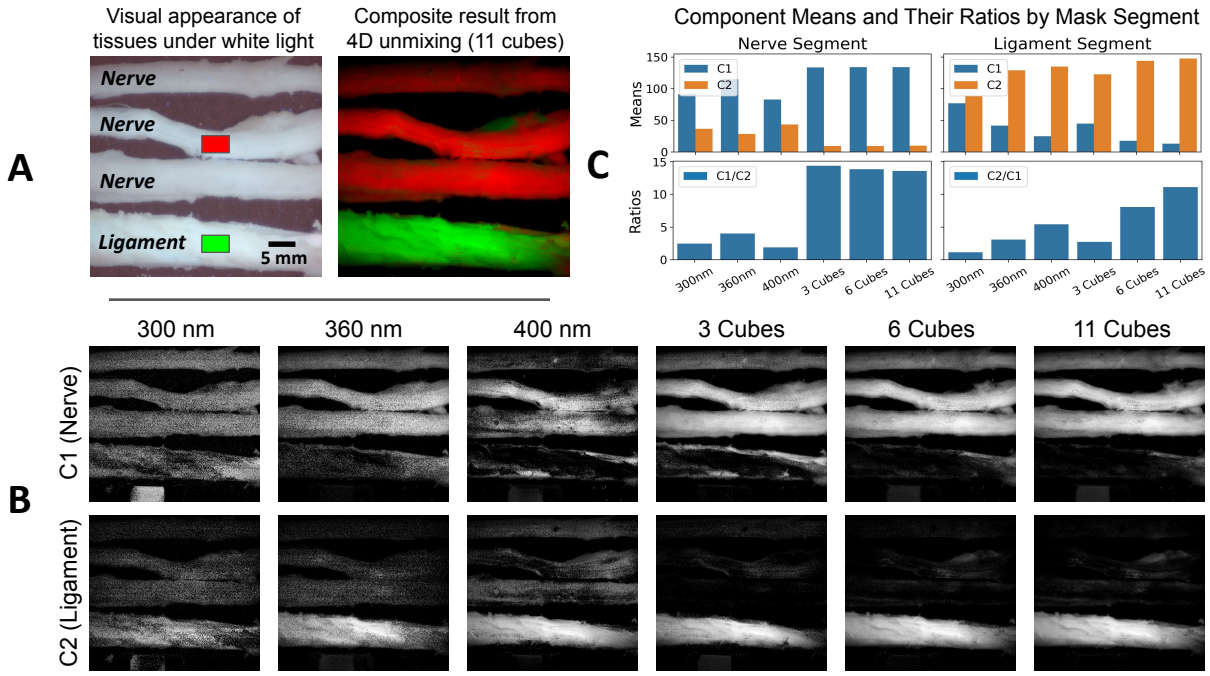

Figure 2: Unmixing results and analysis of 3D vs. 4D HSI configurations. A. Image on the left shows a visual appearance of three nerves (from top to bottom: lateral plantar nerve, medial plantar nerve, peroneal nerve) and the suspensory ligament of the fetlock. Red and green rectangles are the respective ROIs based on which component 1 (C1) and component 2 (C2) spectra were unmixed. The pseudocolor image to the right is a composite image based on unmixing of a 4D HSI dataset composed of eleven 3D HSI cubes acquired under 300 to 400 nm excitation wavelengths in 10 nm intervals. B. The grayscale component images show the relative intensity/quantity of individual component spectra per pixel that the unmixing algorithm has been able to separate the total signal into. For all three tested 4D configurations, the nerve regions had higher density and intensity of component 1. The ligament region had higher density and intensity of component 2 when 6 or 11 different excitation wavelengths were combined into a single 4D HSI dataset. C. Mean intensities of the components within corresponding mask segments and the ratios between them.

Nerves and ligaments from trotters of four adult cows of mixed gender were dissected and imaged. Identical regions of interest were used for extraction of spectra and unmixing steps across all cubes within the same experiment. The unmixing outcomes of individual 3D HSI cubes were inferior to those from multiple 3D cubes combined into one. An illustrative example of one such unmixing study is shown in Fig. 2. The left image of Fig. 2A shows side-by-side the visual appearance of three different excised nerve segments and a ligament. Under incandescent light all four structures appeared white, under UV illumination—all four exhibited broad blue autofluorescence. The composite image on the right was derived after unmixing a 4D dataset stitched from eleven individual 3D cubes with red and green pseudocolor indicating nerve and ligament, respectively. The eleven 420–720 nm cubes were taken using 300 to 400 nm illumination settings in 10 nm intervals, and arranged

sequentially along the emission axis, followed by processing. The grayscale images (Fig. 2B) show component images from processing individual 3D cubes versus the ones derived from the 4D datasets. When the 4D approach is used, the component image intensities are better localized at the corresponding spatial localization of tissues. To derive quantitative results, the mean values of pixel intensity of the two components (Fig. 2B) within nerve and ligament mask segments were compared (Fig. 2C). The data show an increase in the ratio of correctly identified pixels with the increased number of HSI cubes taken at different excitation wavelengths. These ratios, aggregated for all datasets, are presented in Fig. 3B.

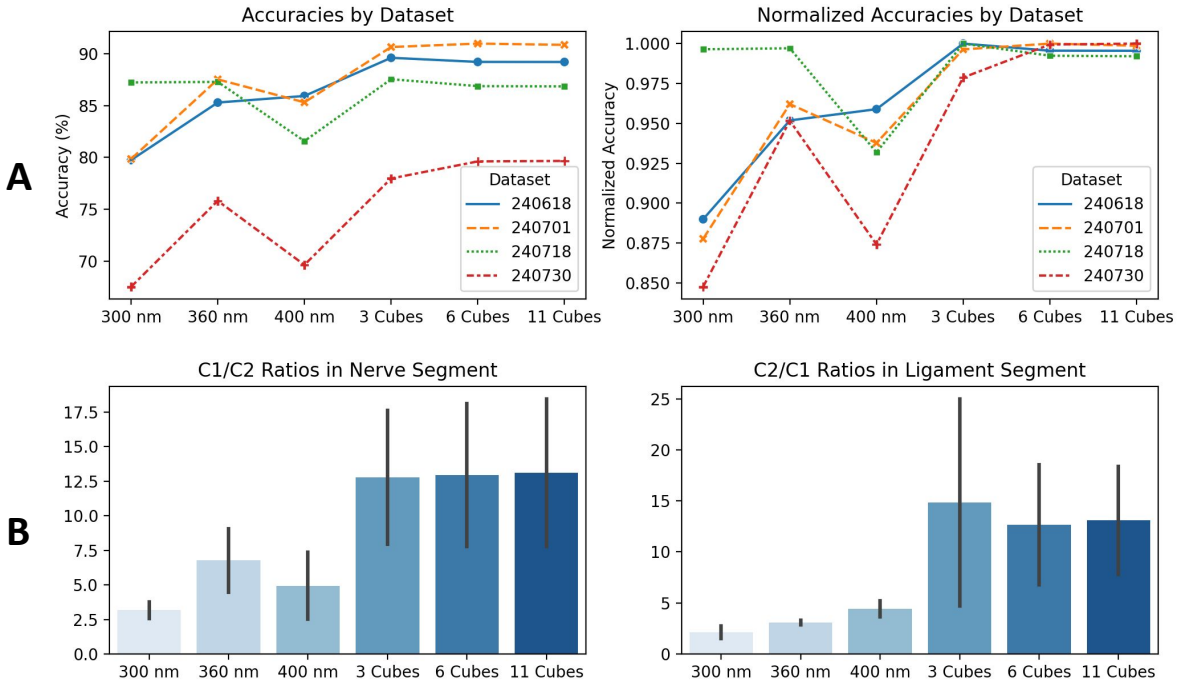

Figure 3: A. Overall accuracies obtained by comparing component-derived masks with reference masks. Values not only increase, but also stabilize with 4D cube configurations. Improvement becomes more evident when comparing data at a similar scale (normalized accuracies). B. Average ratios of component means per mask segment. Error bars stand for standard error.

Additionally, overall accuracy scores indicate improved unmixing outcomes when multiple 3D HSI cubes are combined (Fig. 3A). This improvement is better seen when scores are normalized for each dataset, to bring them to a similar scale (Fig. 3A). For one of the datasets (Fig. 3A, sample 240718, dotted green line) the accuracy exceeded 85% even when a single excitation wavelength, either 300 or 360, was used. Therefore, the engagement of additional excitation wavelengths led to a minimal improvement and this sample was excluded from the statistical calculations shown in Fig. 3B. The Friedman test showed a statistically significant difference between cube configurations in terms of unmixing accuracy ($p = 0.02$).

The accuracy ranges for different datasets suggest that the unmixing outcomes, in general, might depend on the datasets themselves, possibly due to differences in sample or imaging conditions. To overcome this, efforts are needed for data acquisition standardization. However, in the surgical context, neither target tissues nor imaging conditions are subject to fine standardization. This suggests that the focus should primarily be on computational means. In fact, in the companion paper mentioned above,[6] it is shown that CNNs trained on similar ROIs yield higher accuracies than linear unmixing.

In addition to improving the identification of the two target structures, the use of multiple excitations allows to reveal additional features within the view. A clear example of this can be seen in Fig. 4A showing a segment of nerve with a torn epineurium. The damaged area became evident from unmixing a 420–720 nm cube taken

at 325 nm illumination. At longer excitation wavelengths the spectral difference between the two areas becomes less prominent. Yet, when 325 and 385 nm cubes are used in combination, the outcome of unmixing is better than from the 325 nm cube alone. Spectra shown in Fig. 4B illustrate how this effect becomes possible. The top graphs show the raw unnormalized spectra from two regions of interest marked in blue and yellow. During the processing of hyperspectral data, the raw spectra must be normalized in order to distinguish different types of material rather than their amount. Upon normalization the spectral difference between the yellow and the blue ROIs becomes smaller (325 nm) or even negligible (385 nm). However, when the two cubes are stitched together and then normalized, the difference between the two spectral profiles actually increases, leading to better unmixing outcomes.

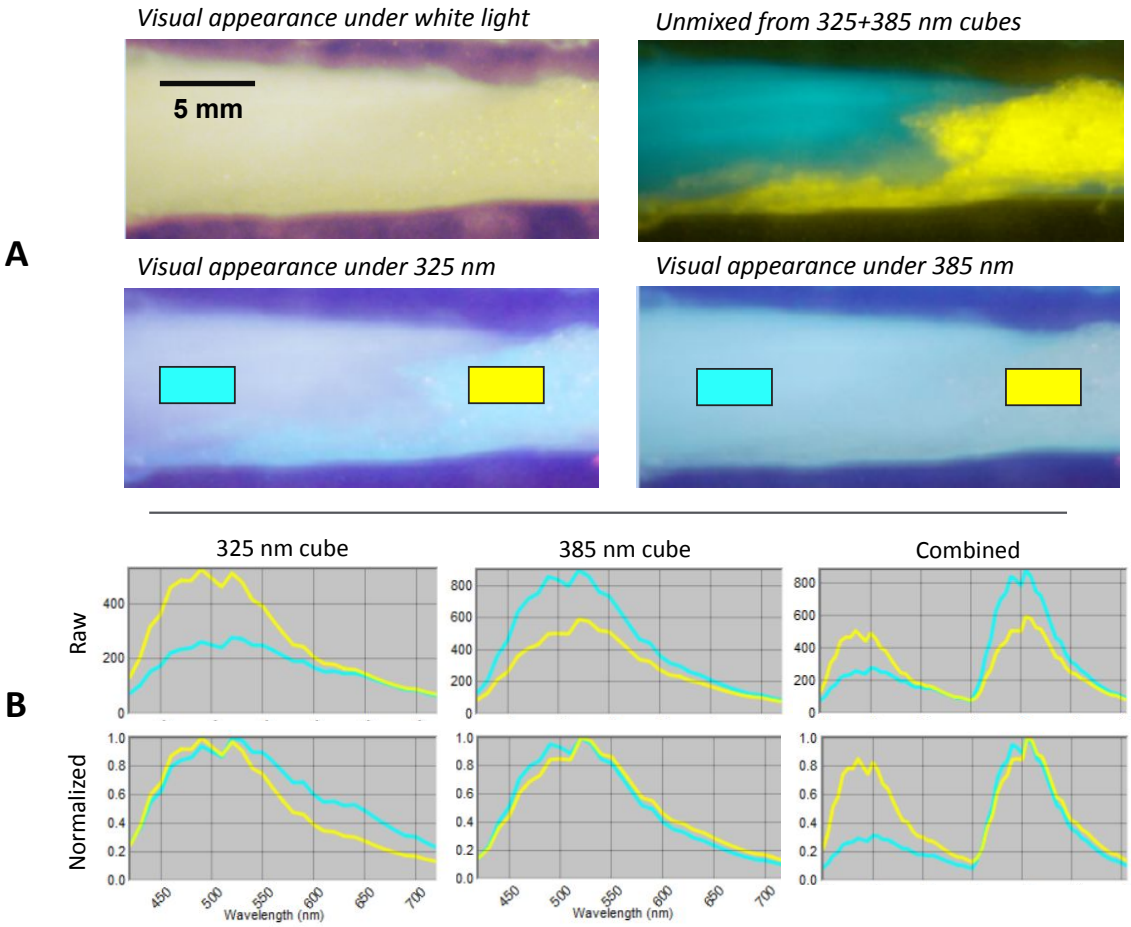

Figure 4: Mechanism behind the increased capacity of 4D HSI approach to reveal spectral differences. A. Top left: Visual appearance of damaged nerve with torn epineurium. Top right. Composite image showing damaged part of the nerve in yellow. The lower two images show the visual appearance of the nerve at 325 and 385 nm illumination settings with two regions of interest from which spectra below were taken. B. The top row shows the raw traces extracted from individual cubes and two cubes stitched together. The bottom row shows the respective normalized spectra.

This report focuses specifically on autofluorescence-based 4D HSI datasets and linear unmixing. However, this modality could be further enhanced by incorporating a reflectance-based HSI dataset into the stack of 3D cubes acquired under UV illumination. This can be easily accomplished by acquiring an additional 3D HSI cube using a broadband illumination source at the end of each experiment. Since ligaments and nerve fibers are both whitish in appearance, adding reflectance data to distinguish them from each other offers minimal benefits.

However, for other anatomical structures within the surgical view, such as blood or lymphatic vessels, reflectance data can be highly beneficial as they introduce complementary information about the color of the target tissue.

4. CONCLUSION

The 4D HSI modality expands the traditional hyperspectral imaging (3D HSI) approach into the second spectral dimension allowing detailed spectroscopic characterization of tissues through the acquisition of excitation–emission matrices from each pixel of an image. Future 4D HSI applications could include a variety of clinical targets such as surgical treatment of internal organs, dental applications, cancerous lesion identification, and other medical procedures where changes in the spectral properties of tissues are anticipated. The presented data strongly suggest that the 4D HSI modality can reveal subtle differences between targets with significantly higher sensitivity than traditional excitation-only or emission-only HSI approaches.

ACKNOWLEDGMENTS

We are grateful to Ani Avetisyan for consultations regarding Nuance FX software and to Vahan Grigoryan for consultations in surgical aspect of the experiments. Financial support of the European Union (NAR-SAR-IPH-101087403) and Afeyan Family Foundation AUA Research Grant Program is gratefully acknowledged. This research has benefited from the Armenian Fellowships Program of the H. Hovnanian Family Foundation, the Short Term Conference and Travel Grant of the Calouste Gulbenkian Foundation, the SPIE Student Conference Support program, and the Professional Development Program of the American University of Armenia in 2025.

REFERENCES

[1] Jacques, S. L., "Optical properties of biological tissues: a review," *Physics in Medicine & Biology* **58**(11), R37 (2013).

[2] Throckmorton, G. A., Haugen, E., Thomas, G., Willmon, P., Baba, J. S., Solórzano, C. C., and Mahadevan-Jansen, A., "Label-free intraoperative nerve detection and visualization using ratiometric diffuse reflectance spectroscopy," *Scientific Reports* **13**(1), 7599 (2023).

[3] Gil, D. A., Swift, L. M., Asfour, H., Muselimyan, N., Mercader, M. A., and Sarvazyan, N. A., "Autofluorescence hyperspectral imaging of radiofrequency ablation lesions in porcine cardiac tissue," *Journal of Biophotonics* **10**(8), 1008–1017 (2017).

[4] Langhout, G. C., Kuhlmann, K. F., Wouters, M. W., van der Hage, J. A., van Coevorden, F., Müller, M., Bydlon, T. M., Sterenborg, H. J., Hendriks, B. H., and Ruers, T. J., "Nerve detection during surgery: optical spectroscopy for peripheral nerve localization," *Lasers in Medical Science* **33**, 619–625 (2018).

[5] Antoniadis, G., Kretschmer, T., Pedro, M. T., König, R. W., Heinen, C. P., and Richter, H.-P., "Iatrogenic nerve injuries: prevalence, diagnosis and treatment," *Deutsches Ärzteblatt International* **111**(16), 273 (2014).

[6] Matosyan, N., Chilingaryan, N., Sarvazyan, N., and Yeghiazaryan, V., "Spectral pixels as images: CNN-based pixel classification of 4D hyperspectral data for nerve and ligament differentiation," in [*Medical Imaging 2025: Image Processing*], SPIE (2025).